PROCEEDINGS, 50th Workshop on Geothermal Reservoir Engineering
Stanford University, Stanford, California, February 10-12, 2025
SGP-TR-229

Insights into the Geochemical Characteristics of Fe-rich Siliceous Scale Deposits Precipitated from Geothermal Water on Atmospheric Silencers at the Menengai Geothermal Field, Kenya

Leakey O. Auko[1,2], Kotaro Yonezu[1], Takushi Yokoyama[3], Saefudin Juhri[1], Jeremiah Kipngok[2], Stephen Onyango[2]

[1]Kyushu University, Dept. Earth Resources Engineering, Fukuoka 819-0395, Japan

[2]Geothermal Development Company, P.O.Box 17700 – 20100, Nakuru, Kenya

[3]Kyushu University, Dept. Chemistry, Fukuoka 819-0395, Japan

leakeyochieng@gmail.com or auko.leakey.855@s.kyushu-u.ac.jp

Keywords: Siliceous, silicic acid, adsorption, amorphous, ferric silicate

ABSTRACT

Siliceous scale deposits retrieved from two atmospheric silencers at the Menengai geothermal field have been chemically and mineralogically characterized to provide insights into understanding the formation mechanisms of the scales under the prevailing atmospheric conditions of about 90-94°C. The scale samples characteristics were studied by XRF, XRD and reflected light microscopy. The chemistry of geothermal water, from which the scale precipitates, is generally alkaline pH with a range of 8.6 to about 10 and is predominantly of HCO_3 or HCO_3-Cl type. Silica concentration ranges between 500 and 1500 mg/kg. The geothermal water also contains high aqueous H_2S levels, ranging from 200 to about 800 ppm. The concentration of Fe and Al is <0.1 and about 0.1 to 0.6 mg/kg respectively. The bulk chemical composition of the scale samples I and II typically suggests that they are iron-rich siliceous deposits where 74 and 77% is SiO_2, and 4 and 12% is total iron, with a corresponding bulk molar ratio of Si:Fe of 24.3 and 8.4, respectively. The enrichment factor for sample I follows the sequence of Fe>Mn>Mg>Ca>Al whereas that of sample II follows the order of Fe>Ca>Mg>Al>Mn. The mineral composition of the two siliceous scale samples consists mainly of amorphous silica, quartz, Fe oxides-oxyhydroxides, boehmite, native sulfur, metal sulfides (pyrite, chalcocite), and halite. Two fundamental formation mechanisms can be deduced, in which coexisting species of Fe and Al competitively participate in scale formation, leading to: (1) the formation of amorphous ferric silicate and (2) the formation of boehmite and amorphous aluminosilicate. The adsorption of silicic acid by ferric hydroxide drives the formation of amorphous ferric silicate. Conversely, the Menengai alkaline water suitably precipitates boehmite (AlOOH) through the absorption of aluminate ion $(Al(OH)_4)^-$ on silicic acid ($Si(OH)_4$) or monosilicate ion $Si(OH)_3O^-$, where boehmite can precipitate either as a residual product or competitively coprecipitates with aluminosilicate.

1. INTRODUCTION

Precipitation of siliceous scale from geothermal brine upon flashing steam and/or cooling on fluid handling equipment is a common phenomenon that invariably poses intricate utilization challenges in most geothermal plants globally. Siliceous scales may form deposits in geothermal- and petroleum-produced waters, desalination plants, and cooling water applications, despite engineering designs and operations potentially predicting that the fluids would not be scale-forming (Gallup and von Hirtz, 2015).Generally, before harnessing the geothermal resource, the aquifer is usually characteristically saturated with respect to quartz and other silica-bearing minerals (Manceau and Gallup, 2005; von Hirtz, 2025). Perturbations occasioned by depressurization boiling can typically result in precipitation of amorphous silica or metal silicates on the surface equipment. Depending on the geothermal brine source, silica scaling is often exacerbated by the presence of calcium, magnesium, iron, aluminum, and manganese metal ions (Kristmannsdóttir, 1989; Manceau and Gallup, 2005; Todd and Bluemle, 2022; von Hirtz, 2025). Aluminum-rich and iron-rich amorphous silicates are the most common and exhibit significantly lower solubilities than pure amorphous silica and have been reported in various geothermal fields globally (Fukuyama and Chen, 2021; Gallup and Reiff, 1991; Juhri et al., 2023; Manceau et al., 1995; Nishida et al., 2009; Todd and Bluemle, 2022; von Hirtz, 2025; Wanyonyi et al., 2024; Yokoyama et al., 1993). Notably, iron-rich siliceous deposits in fluid handling equipment pose undesirable challenges in the utilization of geothermal that have been extensively studied for the mode of formation and suitable countermeasures (Gallup, 1989; Gallup and von Hirtz, 2015; von Hirtz, 2025) . Iron-and aluminum-rich amorphous silica scales typically deposit at much higher temperatures and rates than pure amorphous silica scales (Gallup, 1998). Moreover, besides pure amorphous silica and/or metal-rich amorphous silica, metal sulfides, metal oxides and native elements or alloys have been reported depositing as scales at the wellhead, open canal, separator, heat exchangers, two-phase pipes, and/or reinjection pumps in several geothermal systems (Gallup and Reiff, 1991; Juhri et al., 2023; Reyes et al., 2003).This forms the basis of this study, which aims to provide insights into the characteristics and formation mechanism of the selected-scale deposits retrieved from the Menengai geothermal field situated in the central rift valley in Kenya (Figure 1).

Although silica scaling is not an operational challenge in Menengai, few depositions have been encountered on fluid handling equipment during routine maintenance of the steam gathering system. This study delves into the chemical and mineralogical characteristics of the siliceous precipitate retrieved from two selected silencers at the Menengai geothermal field. Menengai is an elliptical caldera situated in the Kenya Rift. It is the third geothermal field in Kenya to tap and generate electricity after Olkaria and Eburru. A 105MW project is underway in Menengai, with the first 35W built, owned, and operated by the first Independent Power Producer, already transmitted to the national grid (Omenda et al., 2025).

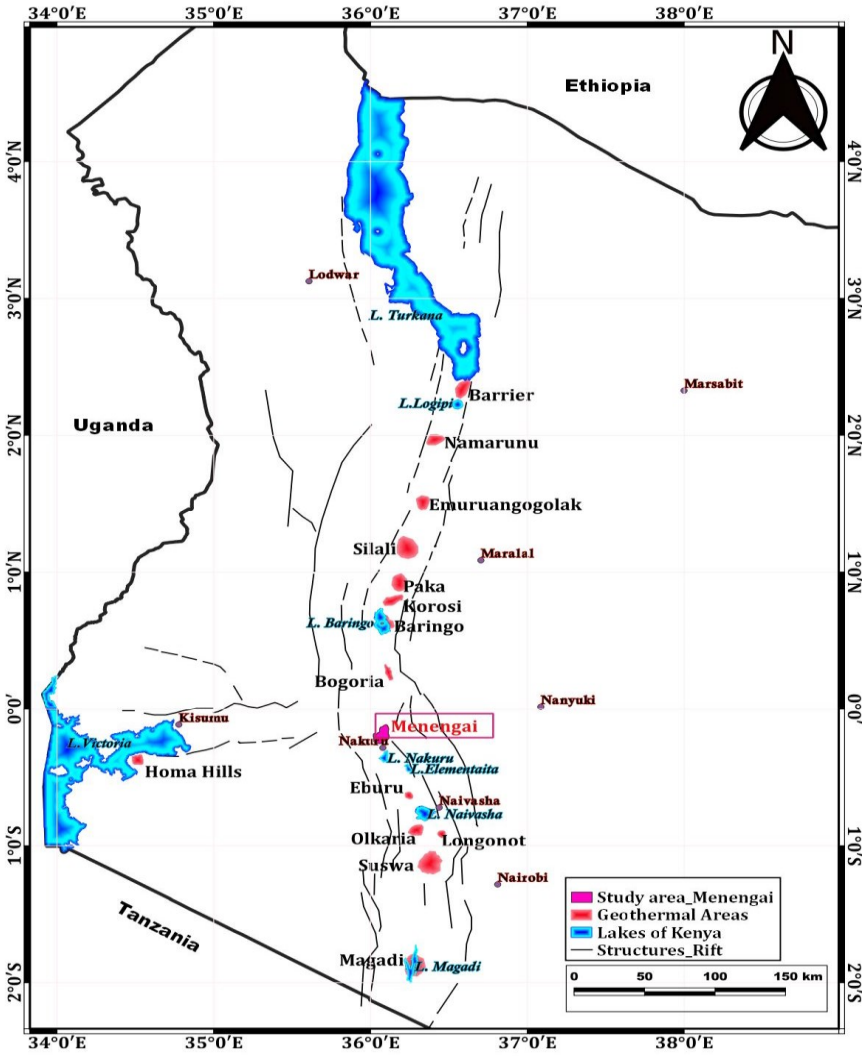

Figure 1: Location of Menengai in the Central Kenya Rift, Nakuru County, (modified after Hochstein and Kagiri, 1997)

The 105 MW output is primarily sustained by high-enthalpy wells sourced from a high-temperature geothermal resource. Reservoir temperatures reaching 400°C at a depth of 2000 m have been recorded in several wells, with four wells encountering molten rhyolitic magma at depths spanning between 2100 and 2300 m within the summit area of the caldera (Omenda et al., 2025). The current steam field configuration for power generation in Menengai is sustained by four centralized vertical production separators coupled with bypass silencers and shared by more than one well. Additionally, two wells each have their individual separators, equipped with a bypass silencer. When geothermal two-phase flow is intermittently channeled through the silencer vessel, steam, and water are separated by cyclone action (Harwood and Hunt, 2014). The steam is usually vented quiescently to the atmosphere, while water flows gravitationally through a duct at the base of the silencer vessels, which is coupled with stacked trachytic rocks and a weir box. NCG's such as H_2S and CO_2 are preferentially expelled into the steam phase in the atmosphere. These perturbations consequently lead to a decrease in temperature (90-94°C), an increase in pH of the residual water circulating in the vessel then becomes supersaturated with silicic acid, $Si(OH)_4^0$ and other ions present in solution (Brown, 2011; Hurwitz et al., 2024). Consequently, depositions have progressively precipitated along the fluid pathway, including the water duct, stacked rocks, walls of the weir box, and the canal leading to the sump. The deposits retrieved from two bypass silencers are christened herein as samples I and II. In this study, the characteristics of the scale samples I and II were evaluated using various complementing analytical methods such as XRF, XRD and reflected light microscopy on polished sections. This was done to understand the formation mechanisms of the scales under the prevailing conditions at 94°C.

2. METHODOLOGY

The bulk chemical composition of major and trace elements in the scales was determined by the X-ray fluorescence (XRF) using a Rigaku ZSX Primus IV XRF machine. The samples were pulverized in a milling machine to prepare a fine homogenous powder and compressed into firm pellets for XRF analysis. Loss on Ignition (LOI) was systematically determined by thermogravimetric method using 1 g of the sample placed in a crucible. The sample was initially heated in a drying oven at 105°C and then heated again in a NIT 10 Kagaku electric furnace sequentially from 500 to 1000°C. Conversely, the mineralogy of scale samples pulverized in the agate motor was determined by X-ray diffraction (XRD) using a Rigaku Ultima IV machine equipped with a Cu-Kα radiation source (40 kV and 20 mA) with a continuous

scanning mode from 2–65° 2θ and a step of 0.02/2θ. Polished sections were also prepared to observe minerals under reflected light microscope and SEM-EDX.

3. RESULTS

3.1 General Chemistry of Geothermal water from which the Scale Precipitate

The chemistry of the geothermal water from Menengai has been previously studied to understand the origin of the fluids and the physicochemical processes in the reservoir (Kipngok et al., 2019; Montcoudiol et al., 2019; Sekento, 2012). Evaluation of fluid chemistry skewed towards silica scaling tendency in a few wells in Menengai MW-20, MW-01 and MW-12 for purposes of direct use was done by Ng'ethe and Jalilinasrabady (2023). The data on the chemistry of the geothermal water synthesized in this study is derived from the 2023-2024 analytical data provided by the Geothermal Development Company, which is consistent with the time of formation or retrieval of scale samples I and II. The chemistry of geothermal water, from which the scale precipitates, is generally alkaline, with a pH range of 8.6 to about 10, and is predominantly of the Na-HCO_3 or Na-HCO_3-Cl type. Silicic acid concentration ranges from 500 up to 1500 mg/kg. Aqueous H_2S levels range from 200 to about 800 mg/kg. Fluoride is about 100 to 600 mg/kg. Na and K spans between 1000 -5000, 100-800 mg/kg respectively whereas Ca is generally low constituting <0.5mg/kg. Mg and Mn is present in trace amounts ranging between 0.01-0.05. Notably, the concentration of Fe and Al in Menengai geothermal water is <0.1 and about 0.1 to 0.6 mg/kg respectively, which is consistently analogous to some of the geothermal water precipitating siliceous scale i.e, in Hatchobaru Japan (Yokoyama et al., 1993), Krafla and Reykjanes (Kristmannsdóttir, 1989), and Olkaria (Wanyonyi et al., 2024).

3.2 Physical description of the scale deposit

Sample I and Sample II were both collected from the base of the bypass silencer vessels with a possible precipitation temperature of 90-94°C. Sample I, appears as mid-tone grey whereas sample II occurs as olive grey with white/yellowish banding possibly pointing to an episodic deposition regime. In addition, the two samples formed sludge on the surface of the vessels. Removal of these scales during routine maintenance was conveniently possible through mechanical high-pressure water jetting.

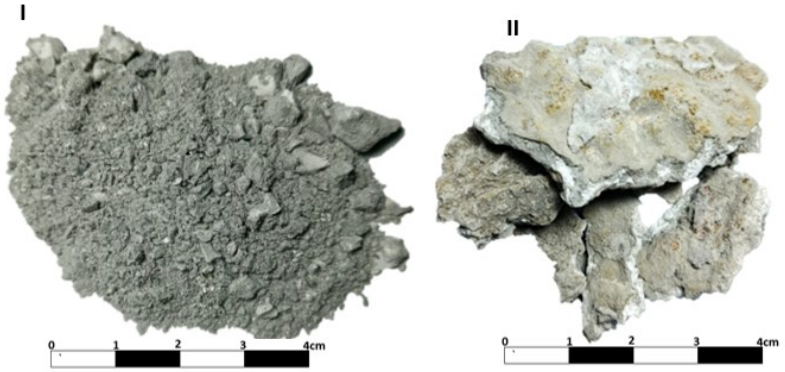

Figure 2: Hand specimen of scale sample I and sample II

3.3 Microscope

Upon examination of the two polished samples under the reflected light microscope (Figure 3), the generated photomicrographs dominantly show gray-colored (sample I) and dark-colored (sample II) subidiomorphic agglomerates of an amorphous groundmass within which large and euhedral to subhedral magnetite grains are randomly interspersed. In addition, in sample II patches of goethite appears to be zoning magnetite.

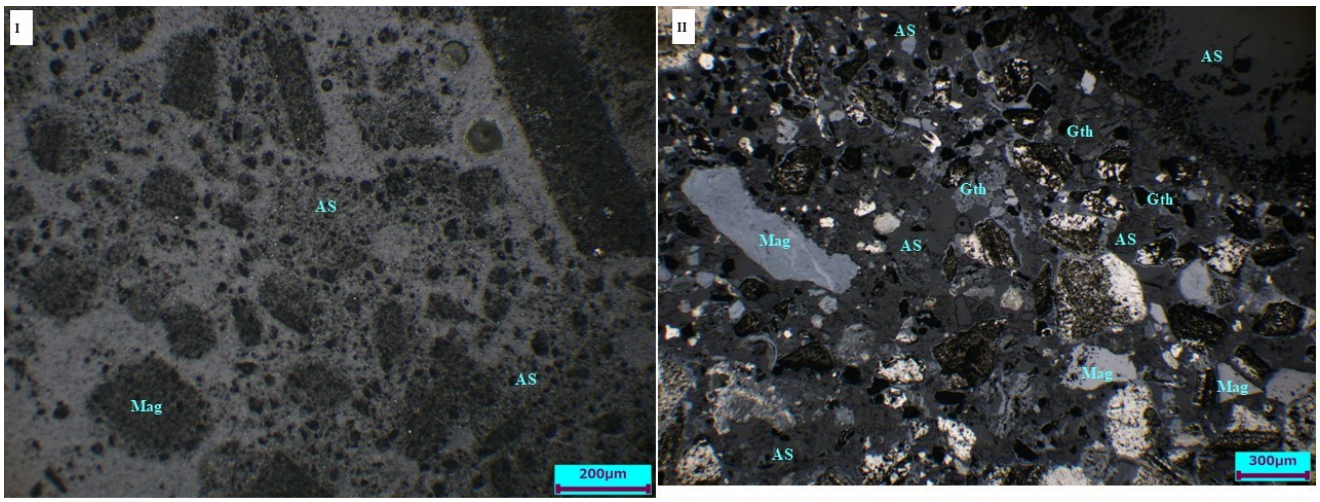

Figure 3: Photomicrographs in the reflected light of a polished section of the silica scale samples I and II showing Amorphous silica (AS), Magnetite (Mag), and Goethite (Gth).

3.4 Bulk chemical composition of the scale deposits

The Sample I scale consists of 74.6% SiO_2, 4.1% Fe_2O_3 (as total Fe), 0.5% Al_2O_3 and 0.2% MgO with a corresponding molar ratio of Si:Fe, Si:Al, Si:Mg of 24.3, 128.1 and 326.9 respectively. On the other hand, the sample II scale consists of 77.6% SiO_2, 12.3% Fe_2O_3 (total Fe), 1.15% Al_2O_3 and 0.2% MgO with a corresponding molar ratio of Si:Fe, Si:Al, Si:Mg of 8.4, 57.35 and 285.98 respectively as shown in Table 1. There is a general incongruence between the scale chemistry and that of the geothermal water precipitating the deposits, as the siliceous deposits are enriched in iron despite the low concentrations of iron i.e. <0.1mg/kg typically present in Menengai geothermal water from which the scales deposit. This is akin to other geothermal fields (Juhri et al., 2023; Kristmannsdóttir, 1989; Yokoyama et al., 1993). Trace amounts of metal cations notably Fe and Al present in geothermal water have a significant capability of forming metal-rich silicate (Gallup, 1997; Yokoyama et al., 1993). However, the enrichment of iron into the siliceous scale due to corrosion products from the steel may not be discounted. In addition, appreciable concentrations of sulfur, chloride, alkali, and alkaline-earth metals are present as shown in Table 1.

Table 1: Bulk chemical composition of the scale deposits (weight %) that were deposited at ~94°C

Constituent	SiO_2	TiO_2	Al_2O_3	Fe_2O_3	MnO	MgO	CaO	Na_2O	K_2O	S	Cl	P_2O_5	LOI	Total
	Concentration (weight %)													
Sample I	74.57	0.08	0.49	4.07	0.05	0.15	0.23	10.78	2.93	0.67	2.57	0.03	5.2	101.8
Sample II	77.60	0.15	1.15	12.31	0.12	0.18	0.25	1.28	0.57	2.04	*bdl*	0.04	5.3	101.0

3.4.1 Enrichment Factor (EF)

The Enrichment Factor is premised on the comparative concentration of the element in the scale deposit relative to its concentration in the geothermal water with respect to silica. The Enrichment Factor (EF) values were calculated as per Equation 1 below adopted from (Yokoyama et al., 1993).

$$E = \frac{([E_S]|[Si_S])}{([E_w]|[Si_w])} \quad (1)$$

Where, Es/Sis and Ew/Siw represent the element/Si molal concentrations in the siliceous scale and geothermal water respectively.

If the Enrichment Factor value of a certain element is larger than 1, it typically indicates the preferential enrichment of the element into the deposit from the geothermal water. Conversely, when the EF is less than 1, it implies that the element didn't participate in the formation of the siliceous scale (Yokoyama et al., 1993). The results of the EF are presented in Table 1. The results show that the enrichment factor for sample I follows the sequence of Fe>Mn>Mg>Ca>Al whereas that of sample II follows the order of Fe>Ca>Mg>Al>Mn.

Table 2: Enrichment factor of elements and corresponding chemical composition of the geothermal waters in which the scale samples precipitated

	Enrichment Factor		Geothermal water chemistry (mg/kg)
Fe	4.3×10^3	1.3×10^4	0.01-0.06
Mn	1.5×10^2	3.4×10^1	0.01 -0.05
Mg	1.1×10^2	1.3×10^2	0.01 -0.05
Ca	3.4×10^1	1.8×10^2	0.05-0.5
Al	2.5×10^1	5.6×10^1	0.1-0.6
K	0.1	0.005	100-800
Na	0.09	0.0002	1000-5000
SiO_2			500-1500

3.5 XRD Mineral Composition

The two scales samples I and II distinctly show a broad scattering hump stretching from 15–30 °2θ and is typically centered at a diffraction angle of about 22-23 °2θ, which is attributable to the amorphous silica and silicate (Manceau et al., 1995; Manceau and Gallup, 2005). In both samples I and II, remarkably weaker peaks of iron minerals (pyrite, magnetite, and goethite) were detected by XRD, typically suggesting that most of the iron was present in amorphous phases. However, small amounts of magnetite and pyrite also existed as crystalline phases. Relatively weaker quartz peaks characterized sample I, whereas sample II is characterized by a markedly sharp peak at 26.65° due to quartz with a corresponding d-spacing of 3.343 Å. An extremely sharp peak around 14.48° and weaker ones at 28.18°, 38.34° and corresponding d-spacing values of 6.112Å, 3.164Å, and 2.346Å respectively, which typically denotes boehmite in sample I, whereas in sample II relatively weaker boehmite peaks are present. The other mineral phases detected in the scale samples by X-ray diffraction include halite, goethite, pyrite, chalcocite, and chabazite as shown in Figure 3.

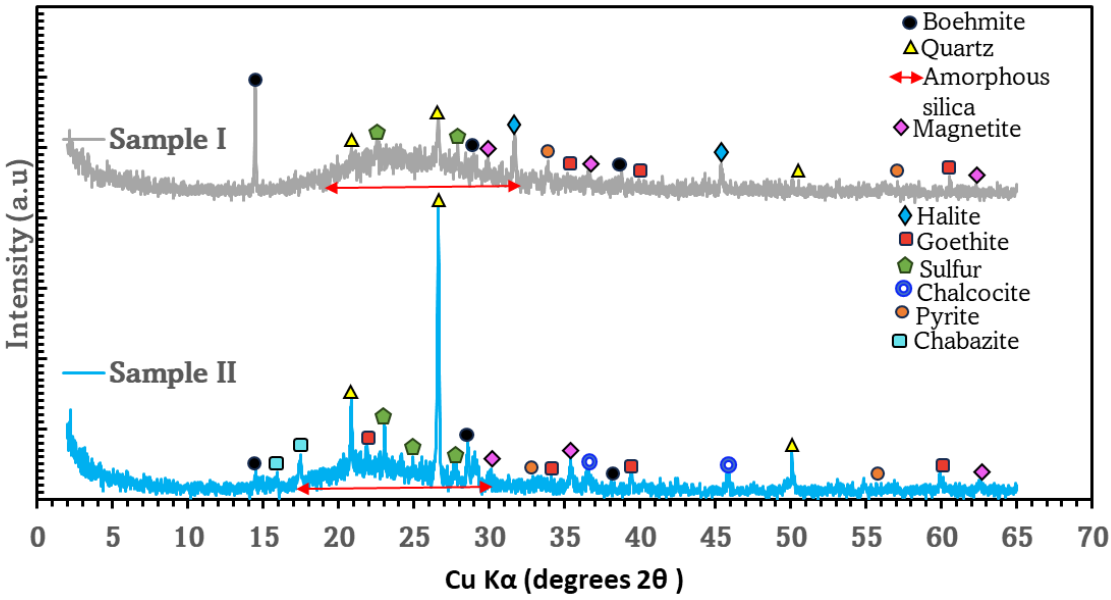

Figure 4: Powder X-ray diffractogram for the scale deposits of sample I and sample II

3.6 Mineral saturation

The saturated state of selected minerals in the geothermal water was calculated with the aid of Geochemist workbench® (Bethke et al., 2024), equipped with the default LLNL thermodynamic database, "thermo.tdat". WATCH speciation code (Arnórsson et al., 1982; Bjarnason, 2010) was used to iteratively model adiabatic boiling of initial aquifer fluid from the reference reservoir temperature down to atmospheric temperature. A summary of the saturation state of selected minerals is presented in Table 2.

Table 3: Saturation state of selected minerals calculated at 94°C for the geothermal water precipitating the silica scale.

Mineral group	Mineral names	Saturation state at 94°C
Silica polymorphs	Amorphous Silica, Quartz	Oversaturated
Fe-silicates	Antigorite, Annite,Daphnite,Minnesotaite, Greenalite,Chamosite, Fayalite, Rhodonite	Oversaturated
Al, Mg-silicates	Phlogopite, Phengite, Talc, Chrysotile, Sepiolite, Saponite-Na, Mordenite-K, Analcime, Clinoptilolite -K Amesite-14A,Sepiolite,Talc	Oversaturated
Sulfur and sulfides	Pyrite, Orpiment, Troilite	Oversaturated
Carbonates	Magnesite, Siderite, Strontianite, Huntite, Calcite, Dolomite, Witherite, Rhodocrosite	Oversaturated
Halides	Fluorite,Sylvite	Undersaturated
Al-hydroxides	Boehmite, Diaspore,Gibbsite	Undersaturated

4. DISCUSSION

4.1 Solubility of amorphous silica and quartz

The most abundant constituent of the siliceous scale deposits is SiO_2. It is therefore very instructive to consider the saturation degree of silicic acid as a measure of the propensity to the formation of siliceous scale deposits. Amorphous silica formation is typically governed by the polymerization rate and the thermodynamic solubility of silicic acid (Brown, 2011; von Hirtz, 2025). The solubility of quartz typically controls the concentration of silicic acid $Si(OH)_4^0$ in the Menengai geothermal reservoir water with temperatures that transcend 300°C. Due to faster precipitation kinetics, among the silica polymorphs, amorphous silica tends to precipitate first (Brown, 2011; von Hirtz, 2025).

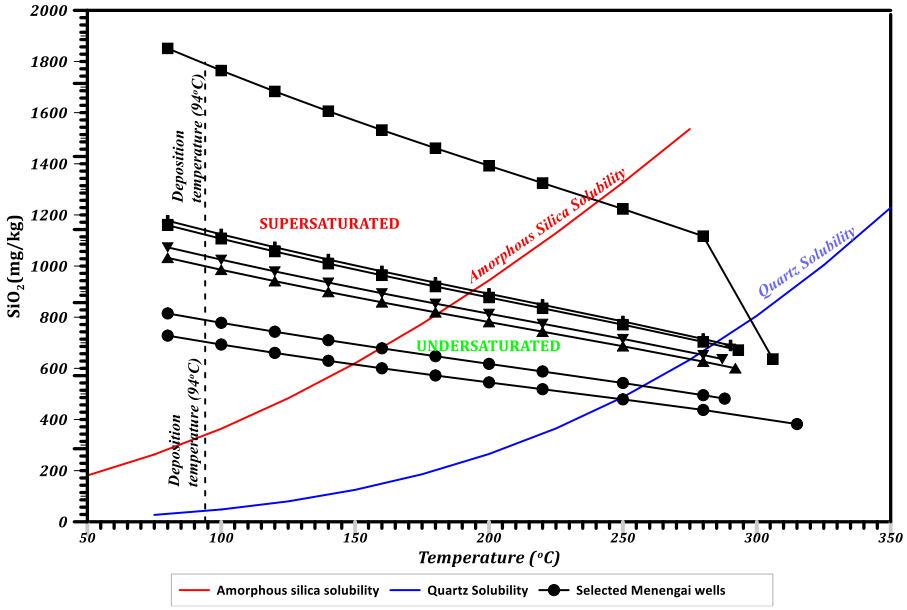

Figure 5: Solubility of quartz and amorphous silica in pure water with temperature, and the solubility of silicic acid upon adiabatic boiling of water from the reservoir temperature to approximately 80°C for selected wells

Figure 4 shows a systematic increase in the solubility of silicic acid upon adiabatic boiling of the water from the reservoir. The Menengai geothermal water is ordinarily silica-supersaturated at the prevailing atmospheric temperature (94°C). The calculated Silica Saturation Index (SSI) exceeds 2 with values of up to 4.5 also computed at 94°C. Once the SSI threshold (SI > 1) is exceeded—i.e., when the monosilicic acid concentration exceeds the solubility of amorphous silica (Chan, 1989; Nishida, 2022) - a rapid process of homogeneous nucleation of nano-colloidal particles is triggered. This leads to the formation of an amorphous silica phase through the polycondensation pathway, producing nanocolloidal particles suspended in the liquid phase, and can grow and undergo ripening, aggregation (coagulation, flocculation), settling, and gelation to transform into solid precipitates (Conrad et al., 2007; Icopini et al., 2005; Iler, 1979; Noguera et al., 2015; van den Heuvel et al., 2018).

Secondly, the Menengai geothermal water is ordinarily saturated in a plethora of silicate minerals and other minerals (sulfides, Fe-oxides). These preexisting minerals laden in geothermal brine provide a substrate for heterogeneous nucleation (van den Heuvel et al., 2018), and initiate the polymerization of silicic acid to form amorphous silica as also reported in other studies (Juhri et al., 2023; Reyes et al., 2003).

The polycondensation of silicic acid reaction in Equation 2 below adopted from Gallup and von Hirtz, (2015), is premised on S_N2 reaction mechanism with steric effect with penta- or hexavalent intermediates/transition states, and backside attack of O- on the Si–OH bond (Issa and Luyt, 2019).

$$2\mathrm{Si(OH)_4} \leftrightarrow (\mathrm{OH})_3Si - O - Si(\mathrm{OH})_3 + \mathrm{H_2O} \qquad (2)$$

The siliceous scales are inherently enrichment in Fe, Al and other alkaline earth elements, and the enrichment factor follows the order of Fe>Mn>Mg>Ca>Al and Fe>Ca>Mg>Al>Mn for samples I and II respectively. The presence of metal ions (e.g. Fe, Al) can significantly accelerate the polycondensation process, since, $Al(OH)_3$ and $Fe(OH)_3$ usually adsorbs large concentrations of silicic acid, thus catalyzing the polycondensation process (Yokoyama et al., 1980, 1989, 1993). It is reported that, pure amorphous silica is seldom the primary scaling candidate in cooling or geothermal systems; instead, metal silicates tend to precipitate at temperatures higher than those predicted for pure amorphous silica, sometimes the precipitation temperature is 25-75 C higher than that for pure amorphous silica (Gallup and von Hirtz, 2015). Section 4.2 highlights the formation mechanism of involving silicic acid and species of Fe and Al.

4.2 Formation mechanisms

Two fundamental formation mechanisms can be deduced, in which coexisting species of Fe and Al competitively participate in scale formation, leading to: (1) the formation of amorphous ferric silicate and (2) the formation of boehmite and amorphous aluminosilicate. Halite may have co-precipitated ostensibly through evaporation, suggesting that it was likely physically incorporated into the siliceous scale deposits rather than actively participating in their formation.

4.1.1 Amorphous Ferric Silicate

XRD analysis typically showed that crystalline iron minerals were detected as very weak peaks in both Sample I and Sample II, despite the high iron content, notably 12% in Sample II. This suggests that iron may dominantly be present in an amorphous state, such as goethite (FeOOH), ferric hydroxide, or ferrisilicate. Ferric ion has been proven to be the more reactive form of iron in the silica precipitation reaction (Gallup, 1998; Yokoyama et al., 1980). Iron (III) hydroxide and aluminum (III) hydroxide have been reported to adsorb large amounts of silicic acid from aqueous solutions and induce silicic acid polymerization to form silica (Iler, 1979; Yokoyama et al., 1980). At a pH of 9 reminiscent of the Menengai geothermal water, maximum amounts of silicic acid are adsorbed by iron (III) hydroxide (Yokoyama et al., 1980). Therefore, assuming the prevalence of ferric hydroxide in the geothermal water circulating in the atmospheric silencers, the formation reactions for amorphous ferric silicate in samples I and II by chemical reactions in Equations 3 and 4 proposed by Gallup (1989) and von Hirtz (2025).

$$Fe(OH)_3 + Si(OH)_4 \rightarrow Fe(OH)_3.SiO_2 + H_2O \quad (3)$$

$$Fe(OH)_3 + Si(OH)_4 + Mg^{2+} \rightarrow Fe(OH)_3.SiO_2.MgO + H_2O + H_2 \quad (4)$$

These reactions are deemed to be very rapid and are presumably the dominant mechanism underpinning the formation of the amorphous ferric silicate matrix in the scale samples. Magnesium may be involved, as indicated by the reaction in Equation 4, due to its high enrichment factor from the bulk composition of the scale sample. Additionally, the formed $Fe(OH)_3 \cdot SiO_2$ or $Fe(OH)_3 \cdot SiO_2 \cdot MgO$ is an amorphous iron (III) silicate that can further act as an adsorption site for silicic acid, depending on the degree of silicic acid supersaturation.

4.1.2 Boehmite and Amorphous Aluminosilicate

The concentration of Al in the geothermal water ranges from 0.1 to 0.6 mg/kg, with Al comprising about 0.5–1% of the scale deposits. XRD diffractogram detected boehmite (AlOOH) in the two scale samples. At a high pH that transcends 9, reminiscent of the Menengai water, silicic acid $Si(OH)_4$ usually deprotonates to liberate $Si(OH)_3O^-$ whereas Al is fundamentally present as aluminate $Al(OH)_4^-$ as shown in Figure 5.

As shown in section 3.6 above, Menengai geothermal water is undersaturated with most aluminium hydroxide minerals, notably boehmite. Sample I, with 4% total Fe, is characterized by a markedly sharp peak of boehmite, whereas in Sample II, with 12% total Fe, boehmite is present with relatively weaker peaks. This may be ascribable to a possible enhanced formation of ferric silicate, which consequently suppresses or slows the hydrolysis of aqueous Al species in the formation environment of sample II. As consistent with the study by Pokrovski et al. (2003), who established that the formation of soluble ferric silicate complexes retards hydrolysis of Al species, and subsequently the nucleation and growth.

The precipitation of boehmite, which is driven by the adsorption of Al species on the surface of silicic acid, can occur either as a residual product or as a competitive coprecipitate alongside amorphous aluminosilicate (Houston et al., 2008; Yokoyama et al., 1989). The possible reactions for the bulk precipitation of boehmite and aluminosilicate, modified from Gallup (1997) within the context of the typical formation mechanisms of aluminosilicate, can be expressed as shown in Equations 5 and 6:

$$3Al(OH)_4^- + Si(OH)_4 \rightarrow Al_2O_3.SiO_2 + AlOOH + 6H_2O + 3OH^- \quad (5)$$

$$3Al(OH)_4^- + Si(OH)_3^- \rightarrow Al_2O_3.SiO_2 + AlOOH + 6H_2O + 4OH^- \quad (6)$$

In addition, Yokoyama et al. (1989) further established that aluminium precipitates on the solid surface as 6-coordinated aluminium hydroxide and a part of the aluminium hydroxide is still even present after the adsorption of monosilicic acid. This residual aluminium hydroxide/aluminate could potentially deprotonate and precipitate boehmite as a secondary product as per Equation 7:

$$Al(OH)_4^- \rightarrow AlOOH + H_2O + OH^- \quad (7)$$

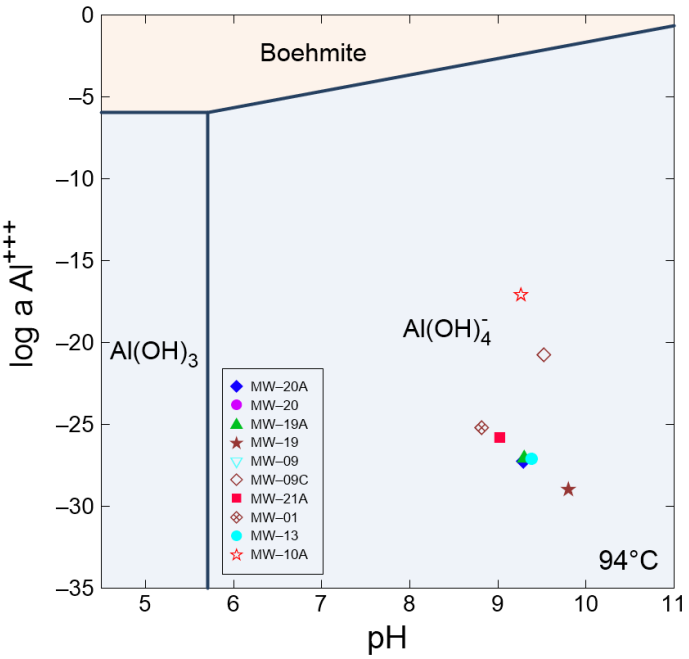

Figure 6: Figure 5: Stability diagram for aluminium species and boehmite at 94°C as a function of pH using The Geochemist's Workbench ® (Bethke et al., 2024). Boehmite was generated after suppressing kaolinite, gibbsite, and diaspore.

5. CONCLUSION

The chemical and mineral composition of the silencer scales samples I and II have been studied. In addition, the formation of silica and other coprecipitating minerals from the geothermal water is also discussed.

- The two siliceous scale samples consist primarily of 74 and 77% SiO_2, while iron constitutes 4% and 12% by weight, with silicon-to-iron (Si/Fe) mole ratios of approximately 24.3 and 8.4, respectively. The enrichment of elements incorporated in the scales follows the order of Fe>Mn>Mg>Ca>Al for sample I, whereas that of sample II follows the sequence of Fe>Ca>Mg>Al>Mn. Iron enriched in the scales is typically derived from the brine, albeit in low concentration. However, the contribution of iron from steel corrosion products to the siliceous scale cannot be ruled out.
- The mineral composition of the two siliceous scale samples consists mainly of amorphous silica and quartz, amorphous hydrous, Fe oxides-oxyhydroxides (magnetite, goethite), boehmite, native sulfur, metal sulfides (pyrite, chalcocite), and halite.
- Amorphous silica formation is premised on a pathway of polycondensation and subsequent deposition as colloidal silica or direct deposition of silicic acid onto solid surfaces (existing saturated minerals silicates, Fe-oxides-oxyhydroxides, sulfides), these minerals provide substrate for the adsorption of silicic acid. Two fundamental formation mechanisms can be deduced where Fe and Al competitively participate in the siliceous scale formation: 1. formation of amorphous hydrous ferric silicate and 2. formation of boehmite and amorphous aluminosilicate.
- The adsorption of silicic acid by ferric hydroxide drives the formation of amorphous hydrous ferric silicate, a process that may be exacerbated at an alkaline pH > 9 reminiscent of Menengai
- The Menengai alkaline water suitably precipitates boehmite (AlOOH) through the absorption of aluminate ion $Al(OH)_4^-$ on silicic acid $Si(OH)_4^0$ or monosilicate $Si(OH)_3^-$ ion, where boehmite can precipitate either as a residual product or competitively, coprecipitates with aluminosilicate.
- Halite may have co-precipitated through evaporation, suggesting that it was likely physically incorporated into the siliceous scale deposits rather than actively participating in their formation

6. ACKNOWLEDGEMENT

We are immensely indebted to the Japan International Cooperation Agency (JICA) KIZUNA program, the LENGO project under the auspices of SATREPS (led by Prof. Fujimitsu, Kyushu University), and the Geothermal Development for the various invaluable roles in supporting this research study.

REFERENCES

Arnórsson, S., Sigurdsson, S., and Svavarsson, H. (1982). The chemistry of geothermal waters in Iceland. I. Calculation of aqueous speciation from 0° to 370°C. *Geochimica et Cosmochimica Acta*, *46*(9), 1513–1532. https://doi.org/10.1016/0016-7037(82)90311-8

Bethke, C. M., Farrell, B., and Sharifi, M. (2024). *The Geochemist's Workbench® -GWB Essentials Guide* (GWB software package Release 17; pp. 1–226). Aqueous Solutions LLC, Champaign, Illinois USA.

Bjarnason, Jón. Ö. (2010). *The Chemical Speciation Program WATCH. Version 2.4* (2.4). Iceland Geosurvey (ISOR) available on https://en.isor.is/software/.

Brown, K. (2011). Thermodynamics and kinetics of silica scaling. *Proceedings International Workshop on Mineral Scaling 2011*, 25–27.

Chan, S. H. (1989). A review on solubility and polymerization of silica. *Geothermics*, *18*(1–2), 49–56. https://doi.org/10.1016/0375-6505(89)90009-6

Conrad, C. F., Icopini, G. A., Yasuhara, H., Bandstra, J. Z., Brantley, S. L., and Heaney, P. J. (2007). Modeling the kinetics of silica nanocolloid formation and precipitation in geologically relevant aqueous solutions. *Geochimica et Cosmochimica Acta*, *71*(3), 531–542. https://doi.org/10.1016/J.GCA.2006.10.001

Fukuyama, M., and Chen, F. (2021). Geochemical characteristics of silica scales precipitated from the geothermal fluid at the Onuma geothermal power plant in Japan. *Journal of Mineralogical and Petrological Sciences*, *116*(3), 159–169. https://doi.org/10.2465/jmps.201130b

Gallup, D. L. (1989). Iron Silicate Scale Formation and Inhibition at the Salton Sea Geothermal Field. *Geothermics*, *18*(1/2), 97–103.

Gallup, D. L. (1997). Aluminum silicate scale formation and inhibition: Scale characterization and laboratory experiments. *Geothermics*, *26*(4), 483–499. https://doi.org/10.1016/S0375-6505(97)00003-5

Gallup, D. L. (1998). Aluminum silicate scale formation and inhibition (2): scale solubilities and laboratory and field inhibition tests. *Geothermics*, *27*(4), 485–501. https://doi.org/10.1016/S0375-6505(98)00024-8

Gallup, D. L., and Reiff, W. M. (1991). Characterization of geothermal scale deposits by Fe-57 mössbauer spectroscopy and complementary x-ray diffraction and infra-red studies. *Geothermics*, *20*(4), 207–224. https://doi.org/10.1016/0375-6505(91)90033-R

Gallup, D. L., and von Hirtz, P. (2015). Control of Silica-Based Scales in Cooling and Geothermal Systems. *Mineral Scales and Deposits: Scientific and Technological Approaches*, 573–582. https://doi.org/10.1016/B978-0-444-63228-9.00022-X

Harwood, K., and Hunt, M. (2014). Prediction of Geothermal Two-phase Silencer Discharge Sound Level. *Proceedings of the 36th New Zealand Geothermal Workshop*, 24–30.

Hochstein, M. P., and Kagiri, D. N. (1997). The role of "steaming ground" over high temperature systems in the Kenya Rift. PROCEEDINGS, Twenty-First Workshop on Geothermal Reservoir Engineering, 29–35. https://www.researchgate.net/publication/267563672

Houston, J. R., Herberg, J. L., Maxwell, R. S., and Carroll, S. A. (2008). Association of dissolved aluminum with silica: Connecting molecular structure to surface reactivity using NMR. *Geochimica et Cosmochimica Acta*, *72*(14), 3326–3337. https://doi.org/10.1016/J.GCA.2008.04.028

Hurwitz, S., Stefánsson, A., Shock, E. L., and Kleine-Marshall, B. I. (2024). The geochemistry of continental hydrothermal systems. *Reference Module in Earth Systems and Environmental Sciences*. https://doi.org/10.1016/B978-0-323-99762-1.00036-X

Icopini, G. A., Brantley, S. L., and Heaney, P. J. (2005). Kinetics of silica oligomerization and nanocolloid formation as a function of pH and ionic strength at 25°C. *Geochimica et Cosmochimica Acta*, *69*(2), 293–303. https://doi.org/10.1016/J.GCA.2004.06.038

Iler, R. K. (1979). *The Chemistry of Silica. Solubility, Polymerization Colloid and Surface Properties and Biochemistry*. John Wiley and Sons.

Issa, A., and Luyt, A. (2019). Kinetics of Alkoxysilanes and Organoalkoxysilanes Polymerization: A Review. *Polymers*, *11*(3), 537. https://doi.org/10.3390/polym11030537

Juhri, S., Yonezu, K., Harijoko, A., Nurpratama, M. I., and Yokoyama, T. (2023). Diverse scale deposition in response to the change in chemical properties of geothermal water at the Dieng geothermal power plant, Indonesia. *Geothermics*, *111*, 102717. https://doi.org/10.1016/J.GEOTHERMICS.2023.102717

Kipngok, J., Auko, L., Malimo, S., Igunza, G., Kangogo, S., Ranka, L., Bett, E., Suwai Janet, and Matsuda Koji. (2019). Geochemical Characteristics of the Menengai Geothermal Reservoir. *GRC Transactions, Vol 43*.

Kristmannsdóttir, H. (1989). Types of scaling occurring by geothermal utilization in Iceland. *Geothermics*, *18*(1–2), 183–190. https://doi.org/10.1016/0375-6505(89)90026-6

Manceau, A., and Gallup, D. L. (2005). Nanometer-sized, divalent-Mn, hydrous silicate domains in geothermal brine precipitates. *American Mineralogist*, *90*(2–3), 371–381. https://doi.org/10.2138/am.2005.1599

Manceau, A., Ildefonse, P., Hazemann, J. L., Flank, A. M., and Gallup, D. (1995). Crystal chemistry of hydrous iron silicate scale deposits at the salton sea geothermal field. *Clays and Clay Minerals*, *43*(3), 304–317. https://doi.org/10.1346/CCMN.1995.0430305

Montcoudiol, N., Burnside, N. M., Györe, D., Mariita, N., Mutia, T., and Boyce, A. (2019). Surface and groundwater hydrochemistry of the Menengai caldera geothermal field and surrounding Nakuru County, Kenya. *Energies*, *12*(16). https://doi.org/10.3390/en12163131

Ng'ethe, J., and Jalilinasrabady, S. (2023). GIS-based multi-criteria decision making under Silica Saturation Index (SSI) for selecting the best direct use scenarios for geothermal resources in Central and Southern Rift Valley, Kenya. *Geothermics*, *109*, 102656. https://doi.org/10.1016/J.GEOTHERMICS.2023.102656

Nishida, I. (2022). Silica and metal silicate deposits. *Water-Formed Deposits: Fundamentals and Mitigation Strategies*, 195–211. https://doi.org/10.1016/B978-0-12-822896-8.00034-0

Nishida, I., Shimada, Y., Saito, T., Okaue, Y., and Yokoyama, T. (2009). Effect of aluminum on the deposition of silica scales in cooling water systems. *Journal of Colloid and Interface Science*, *335*(1), 18–23. https://doi.org/10.1016/J.JCIS.2009.02.050

Noguera, C., Fritz, B., and Clément, A. (2015). Precipitation mechanism of amorphous silica nanoparticles: A simulation approach. *Journal of Colloid and Interface Science*, *448*, 553–563. https://doi.org/10.1016/J.JCIS.2015.02.050

Omenda, P., Ofwona, C., and Mangi, P. (2025). Kenya: The Most Successful Geothermal Development in Africa. *Geothermal Power Generation*, 863–891. https://doi.org/10.1016/B978-0-443-24750-7.00022-1

Pokrovski, G. S., Schott, J., Farges, F., and Hazemann, J. L. (2003). Iron (III)-silica interactions in aqueous solution: insights from X-ray absorption fine structure spectroscopy. *Geothermics*, *67*(19), 3559–3573. https://doi.org/10.1016/S0016-7037(03)00160-1

Reyes, A. G., Trompetter, W. J., Britten, K., and Searle, J. (2003). Mineral deposits in the Rotokawa geothermal pipelines, New Zealand. *Journal of Volcanology and Geothermal Research*, *119*(1–4), 215–239. https://doi.org/10.1016/S0377-0273(02)00355-4

Sekento, L. R. (2012). Geochemical and Isotopic Study of the Menengai Geothermal Field, Kenya. In *United Nations University - Geothermal Training Program, Report No.31, Reykjavik-Iceland* (pp. 769–792).

Todd, M. A., and Bluemle, M. J. (2022). Formation and mitigation of mineral scaling in geothermal power plants. *Water-Formed Deposits: Fundamentals and Mitigation Strategies*, 269–282. https://doi.org/10.1016/B978-0-12-822896-8.00002-9

van den Heuvel, D. B., Gunnlaugsson, E., Gunnarsson, I., Stawski, T. M., Peacock, C. L., and Benning, L. G. (2018). Understanding amorphous silica scaling under well-constrained conditions inside geothermal pipelines. *Geothermics*, *76*, 231–241. https://doi.org/10.1016/J.GEOTHERMICS.2018.07.006

von Hirtz, P. (2025). Silica Scale Control in Geothermal Plants: Historical Perspective and Current Technology. *Geothermal Power Generation*, 497–531. https://doi.org/10.1016/B978-0-443-24750-7.00014-2

Wanyonyi, E., Yonezu, K., Imai, A., Yokoyama, T., Opondo, K., and Koech, K. (2024). Geochemical study on the deposition of silica scale at Olkaria well OW-35: A key to understanding the formation mechanisms of silica scale at the Olkaria Geothermal Field, Kenya. *Geothermics*, *117*, 102871. https://doi.org/10.1016/J.GEOTHERMICS.2023.102871

Yokoyama, T., Sato, Y., Maeda, Y., Tarutani, T., and Itoi, R. (1993). Siliceous deposits formed from geothermal water I. The major constituents and the existing states of iron and aluminium. *Geochemical Journal*, *27*, 375–384.

Yokoyama, T., Takahashi, Y., Yamanaka, C., and Tarutani, T. (1989). Effect of aluminium on the polymerization silicic acid in aqueous solution and the deposition of silica of silica. *Geothermics*, *18*(1–2), 321–326. https://doi.org/10.1016/0375-6505(89)90042-4

Yokoyama, T., Taratuni, T., and Nakazato, T. (1980). Polymerization of silicic acid adsorbed on iron(III) hydroxide. *Bull. Chem. Soc. Jpn*, *53*(4), 850–853. https://doi.org/https://doi.org/10.1246/bcsj.53.850.